JACS
JOURNAL OF THE AMERICAN CHEMICAL SOCIETY

Article

pubs.acs.org/JACS

Aromatic Saddles Containing Two Heptagons

Kwan Yin Cheung,[†] Xiaomin Xu,[†] and Qian Miao*[,†,‡]

[†]Department of Chemistry, The Chinese University of Hong Kong, Shatin, New Territories, Hong Kong, China
[‡]Institute of Molecular Functional Materials (Areas of Excellence Scheme, University Grants Committee), Hong Kong, China

Supporting Information

ABSTRACT: Soluble derivatives of $C_{70}H_{26}$ (**1a,b**) and $C_{70}H_{30}$ (**2a,b**), two new saddle-shaped polycyclic arenes containing two heptagons, were successfully synthesized from saddle-shaped diketones (**3a,b**), whose carbonyl groups are the key in the reactions to extend the polycyclic π-framework. As found from the crystal structures, the polycyclic backbone of **1b** has a deep saddle shape, while that of **2b** is even more distorted because of the existence of two [4]-helicene moieties. On the basis of crystal structures, local aromaticity and nonplanarity of individual rings in the saddle-shaped π-backbone were analyzed, and were found to follow Clar's rule in general. It was found that **1b** and **3b** behaved as p-type semiconductors in solution-processed thin film transistors while the amorphous films of **2b** appeared insulating.

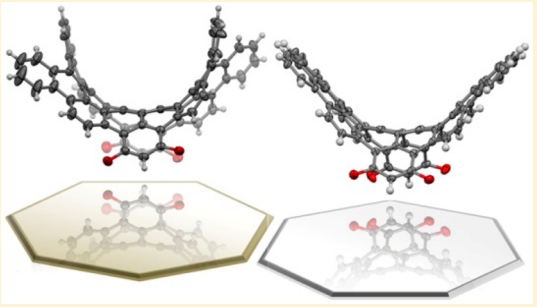

INTRODUCTION

Fullerenes, carbon nanotubes, and graphene are hollow spheres/ellipsoids, straight tubes, and flat sheets of sp^2 carbon atoms, respectively. These conjugated carbon nanomaterials have received tremendous attention and have a very important place in nanoscience owing to their exceptional electrical, thermal, chemical, and mechanical properties. Carbon nanostructures with novel geometry can in principle provide new conjugated carbon nanomaterials with interesting properties. For example, toroidal carbon nanotubes are predicted to have peculiar persistent currents and giant paramagnetic susceptibility.[1] Embedding nonhexagonal rings into a graphitic lattice of sp^2 carbons can force the π-backbones out of planarity to retain the typical C−C bond distances.[2,3] The spherical face of fullerenes have positive Gaussian curvature, while the plane of graphene and the cylindrical face of carbon nanotubes have zero Gaussian curvature. Negatively curved conjugated carbon networks with embedded heptagons were first proposed in 1992 on the basis of calculation,[4] and heptagon-embedded carbon nanotubes of negative curvature were experimentally observed later in the same year.[5] Computational studies suggest that heptagon-embedded graphitic structures with a negative Gaussian curvature have a net magnetic moment,[6] and toroidal carbon nanotubes containing both heptagons and pentagons are thermodynamically stable with lower total energies per atom than C_{60}.[1,7] However, these interesting carbon nanostructures with negative curvature remain imaginary, and heptagon-embedded polycyclic arenes that can serve as segments, model compounds, and in principle, synthetic precursors for them are still rare. Recent approaches to negatively curved carbon nanostructures with saddle-shaped polycyclic arenes[8] include a heptagon-embedded *peri*-hexabenzocoronene (HBC)[9] and $C_{80}H_{30}$, a grossly warped nanographene containing five heptagons.[10] Here we report derivatives of $C_{70}H_{26}$ (**1a,b**) and $C_{70}H_{30}$ (**2a,b**), two new saddle-shaped polycyclic arenes containing two heptagons as shown in Figure 1. The synthetic precursors of **1a,b** and **2a,b** are saddle-shaped diketones (**3a−c**), whose π-backbone is forced out of planarity by inserting two carbonyl groups into HBC. Detailed below are synthesis and structures of **1a,b**, **2a,b** and **3a−c** as well as a brief investigation of semiconductor properties in solution-processed thin film transistors.

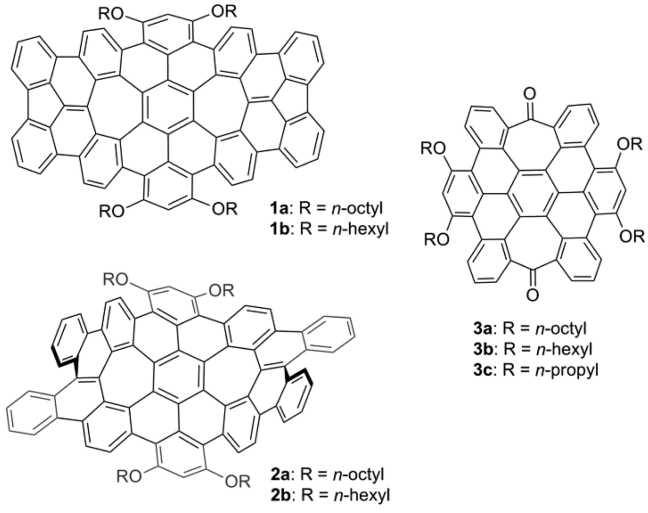

Figure 1. Molecular structures of saddle-shaped conjugated molecules **1a,b**, **2a,b**, and **3a−c**.

Received: January 13, 2015
Published: March 5, 2015

DOI: 10.1021/jacs.5b00403
J. Am. Chem. Soc. 2015, 137, 3910−3914

RESULTS AND DISCUSSION

Synthesis. Shown in Scheme 1 is the synthesis of **3a**–**c** as adapted from the well-known Müllen's synthesis of substituted

Scheme 1. Synthesis of 3a–c[a]

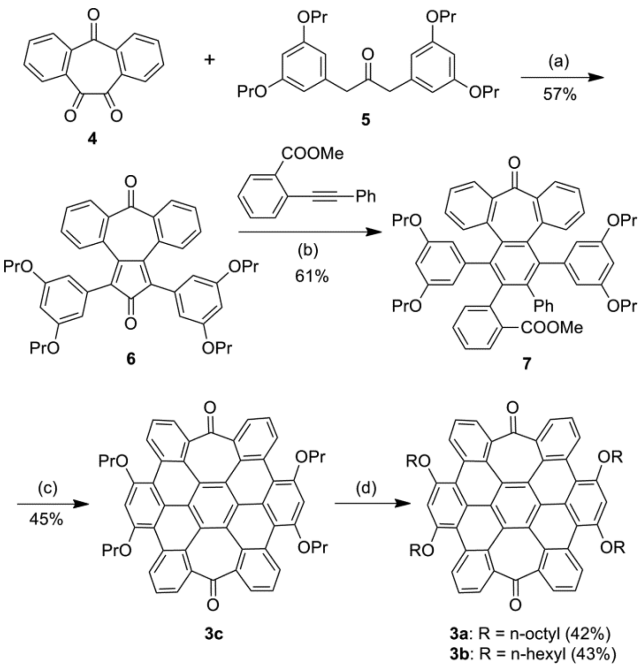

[a]Reagents and conditions: (a) KOH/MeOH, THF; (b) diphenyl ether, reflux; (c) (i) DDQ, CF_3SO_3H, CH_2Cl_2; (ii) CH_3SO_3H; (d) (i) BBr_3, CH_2Cl_2; (ii) K_2CO_3, RBr, DMF.

HBCs[11] including Diels–Alder cycloaddition and oxidative cyclodehydrogenation as the key steps. The first heptagon was introduced from 2,3:6,7-dibenzocycloheptadiene-1,4,5-trione (**4**),[12] which underwent double aldol condensation with 1,3-diphenylacetone **5** yielding heptagon-fused cyclopentadienone **6**. Diels–Alder reaction of **6** followed by decarbonylation gave hexaphenylbenzene derivative **7** as a mixture of conformers due to the restricted rotation of C–C single bonds between benzene rings. A similar synthesis of unsubstituted versions of **6** and **7** was reported decades ago,[13] but almost neglected afterward. Oxidative cyclodehydrogenation of **7** with DDQ and triflic acid and subsequent intramolecular Friedel–Crafts acylation mediated by methanesulfonic acid resulted in diketone **3c** with the second heptagon introduced. The positions of the four alkoxy groups were important to activate the cyclization at the desired position as noted earlier with the synthesis of the heptagon-embedded HBC.[9] The propyl groups of **3c** were then replaced with other alkyl chains yielding **3a**,**b**. The propyl group was chosen as the solubilizing substituent in this synthesis because it not only provided reasonable solubility to **3c** for convenient purification but also, upon dealkylation with BBr_3, resulted in 1-bromoproane, which was easily removed under reduced pressure before the subsequence alkylation.

The conjugated backbone of **3a**,**b** was then extended from the two carbonyl groups by two ways. Scheme 2 shows the synthesis of **1a**,**b** from **3a**,**b**. Nucleophilic addition of fluorene anions to the two carbonyl groups of **3a**,**b** gave diol **8a**,**b**, which was dehydrated under an acidic condition yielding **9a**,**b**. Subsequent oxidative cyclodehydrogenation of **9a**,**b** with DDQ and triflic acid yielded **1a**,**b**. Scheme 3 shows the synthesis of **2a**,**b** from

Scheme 2. Synthesis of 1a,b[a]

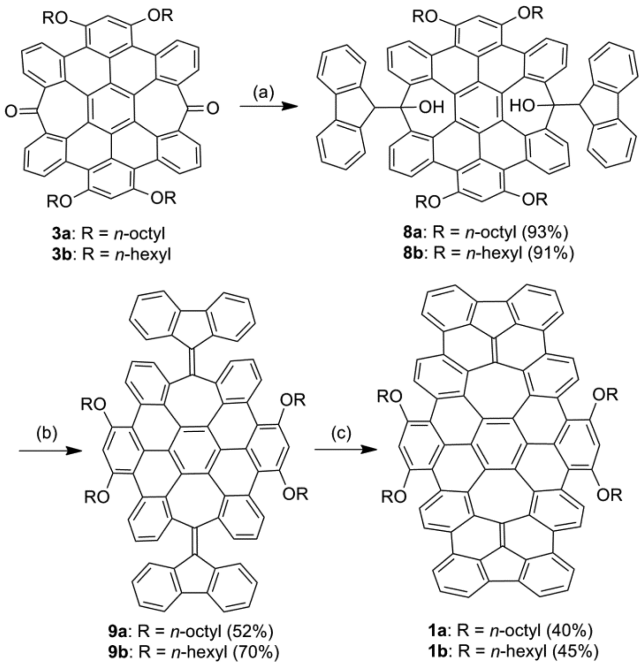

[a]Reagents and conditions: (a) *n*-BuLi, fluorene, THF; (b) TsOH, Ac_2O, toluene; (c) DDQ, CF_3SO_3H, CH_2Cl_2.

Scheme 3. Synthesis of 2a,b[a]

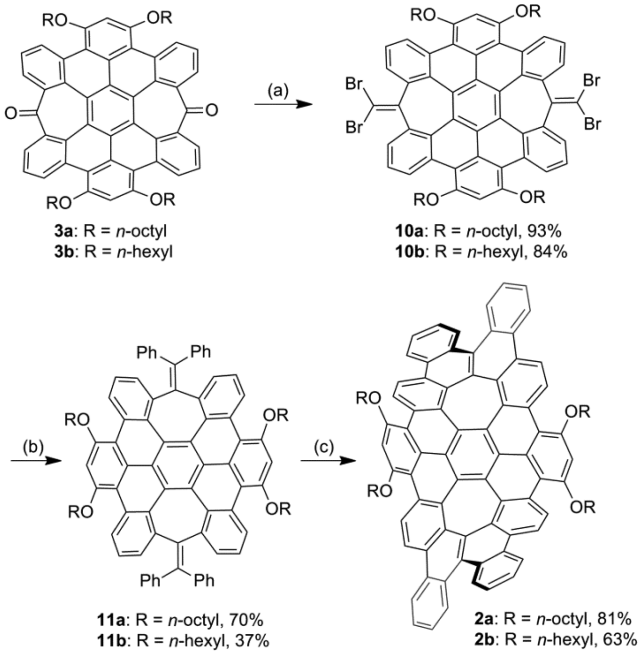

[a]Reagents and conditions: (a) PPh_3, CBr_4, toluene; (b) phenylboronic acid, $Pd(PPh_3)_4$, K_2CO_3, toluene/H_2O/EtOH; (c) DDQ, CF_3SO_3H, CH_2Cl_2.

3a,**b**. The two carbonyl groups of **3a**,**b** reacted with CBr_4 in the Corey–Fuchs reaction to give **10a**,**b**, which, upon Suzuki coupling with phenylboronic acid, led to **11a**,**b**. Oxidative cyclodehydrogenation of **11a**,**b**, in a similar manner as that of **9a**,**b**, yielded **2a**,**b**. Analogues of **1a**,**b** and **2a**,**b** with shorter alkyl chains were not successfully synthesized due to their poor solubility.

DOI: 10.1021/jacs.5b00403
J. Am. Chem. Soc. 2015, 137, 3910–3914

Optical and Electronic Properties. Diketones **3a**–**c** are soluble in common organic solvents resulting in a yellow solution with green fluorescence when irradiated with UV light. In contrast, the orange solutions of **1a**,**b** exhibit very weak fluorescence and the orange solutions of **2a**,**b** appear almost nonfluorescent as shown in Figure S2 (the Supporting Information), likely in relation to the flexibility of their polycyclic backbones. The π-extended polycyclic backbones of **1a**,**b** and **2a**,**b** are more flexible than that of **3a**–**c** and thus allow conformational change (e.g., flapping), which consumes the energy of excited state resulting in radiationless internal conversion. With two [4]helicene moieties, the polycyclic backbone of **2a**,**b** is more flexible than that of **1a**,**b**, leading to almost nonfluorescent solutions. In agreement with this explanation, **1a**,**b** and **2a**,**b** exhibit enhanced fluorescence in the solid state as shown in Supporting Information, Figure S2. This can be attributed to aggregation induced emission (AIE) due to restriction of intramolecular motions.[14] Figure 2 shows the

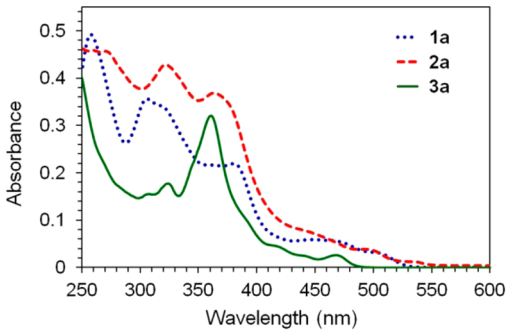

Figure 2. UV–vis absorption spectra of **1a**, **2a**, and **3a** in CH_2Cl_2 (5×10^{-6} mol/L).

absorption spectra of **1a**, **2a**, and **3a** in CH_2Cl_2 at the same concentration. The absorption spectrum of **3a** is very similar to that of the previously reported heptagon-embedded HBC, which has a methylene group in the seven-membered ring.[9] This suggests the two carbonyl groups in **3a** are poorly conjugated with the polycyclic π-framework. Compounds **1a** and **2a** exhibit similar absorptions, which are red-shifted relative to **3a** as well as the previously reported heptagon-embedded HBC, in agreement with the extended π-conjugation. The cyclic voltammogram of **1a** in CH_2Cl_2 exhibits three quasi-reversible oxidation waves with half-wave oxidation potentials of 0.28, 0.43, and 0.56 V vs ferrocenium/ferrocene while that of **2a** exhibits one reversible oxidation wave with half-wave oxidation potentials of 0.27 V vs ferrocenium/ferrocene. The cyclic voltammogram of **3a** in CH_2Cl_2 exhibits two reversible oxidation waves with half-wave oxidation potentials of 0.63 and 0.83 V vs ferrocenium/ferrocene. From the first half-wave oxidation potential, the HOMO energy level of **1a**, **2a**, and **3b** are estimated as −5.38, −5.37, and −5.73 eV, respectively.[15]

Crystal Structures. Single crystals of **2b** and **3b** were grown from solutions in toluene/CH_2Cl_2 and ethyl acetate/CH_2Cl_2, respectively, by slow evaporation of solvents, while single crystals of **1b** were grown by slow diffusion of ethyl acetate vapor into a solution of **1b** in chlorobenzene. The resolved crystal structures of **1b**, **2b**, and **3b** all show disorder of alkyl chains suggesting inefficient filling of space with these saddle-shaped molecules. Therefore, the following discussions on crystal structures are focused on the conjugated backbones. As shown in Figure 3, the saddle-shaped π-backbone of **3b** in the crystal structure is 10.6 Å

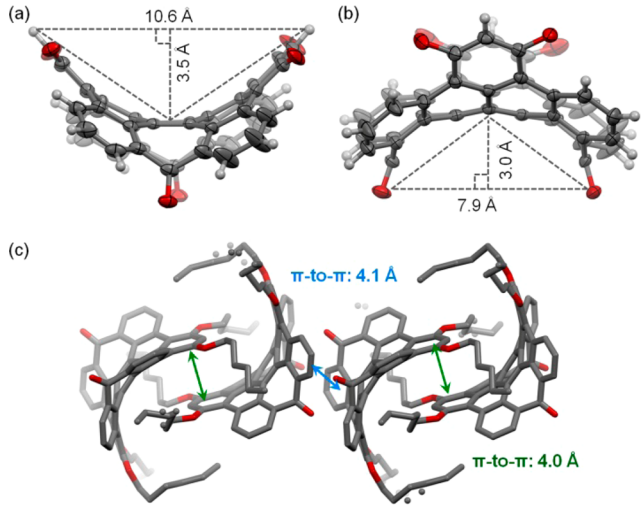

Figure 3. Crystal structure of **3b**: (a) front view and (b) side view of the π-backbone of **3b** with the hexyl groups removed and carbon atom positions shown as 50% probability ellipsoids; (c) molecular packing of **3b** with hydrogen atoms removed for clarity. (Disordered carbon atoms are shown as dots.)

wide and 3.5 Å deep in the upper part, and is 7.9 Å wide and 3.0 Å deep in the lower part. Molecules of **3b** are packed in such a way (shown in Figure 3c) that the alkyl chains occupy the space above the saddle face. This packing motif leads to poor intermolecular π–π interactions with small overlap and large distance (4.0–4.1 Å) between benzene rings.

Shown in Figure 4 panels a and b is the saddle-shaped π-backbone of **1b** in the crystal structure, which is wider and deeper than **3b** in the upper part because of π-extension. Having a bond length of 1.46–1.48 Å, the C–C bonds shown in green are significantly longer than a typical C–C aromatic bond (1.38–1.40 Å) but resemble C–C single bonds between sp^2-sp^2 carbons, which have a typical bond length of 1.45–1.48 Å depending on the degree of conjugation.[16] This is in agreement with localization of π-bonds in the seven-membered ring. The unit cell of **1b** contains two crystallized molecules of water, which are presumably from wet solvents. As shown in Figure 4c, the crystal structure of **1b** exhibits a loose packing of π-backbones with only a few edge-to-face (not shown) short contacts and a large distance (4.2 Å) between parallel benzene rings of neighboring molecules.

As found from the crystal structure, **2b** has an even more curved π-face than **1b** because it contains two [4]helicene moieties besides two seven-membered rings. With its two [4]helicene moieties having the same axial chirality, **2b** is a chiral molecule, which exists as a pair of enantiomers in the crystals. Figure 5 panels a and b show the π-backbone of one enantiomer. The C–C bonds shown in green are 1.46–1.48 Å long resembling C–C single bonds between sp^2-sp^2 carbons,[16] suggesting localization of π-bonds in the seven-membered ring. As shown in Figure 5c, molecules of **2b** are packed more tightly in the crystal than those of **1b** with closer face-to-face contacts (about 3.5 Å) between parallel benzene rings of neighboring molecules.

On the basis of the crystal structures, the curvature of individual rings in the curved π-backbones of **1b** and **2b** was analyzed in terms of nonplanarity, and the local aromaticity of individual rings was analyzed using the harmonic oscillator model of aromaticity (HOMA).[17] The nonplanarity of the

DOI: 10.1021/jacs.5b00403
J. Am. Chem. Soc. 2015, 137, 3910–3914

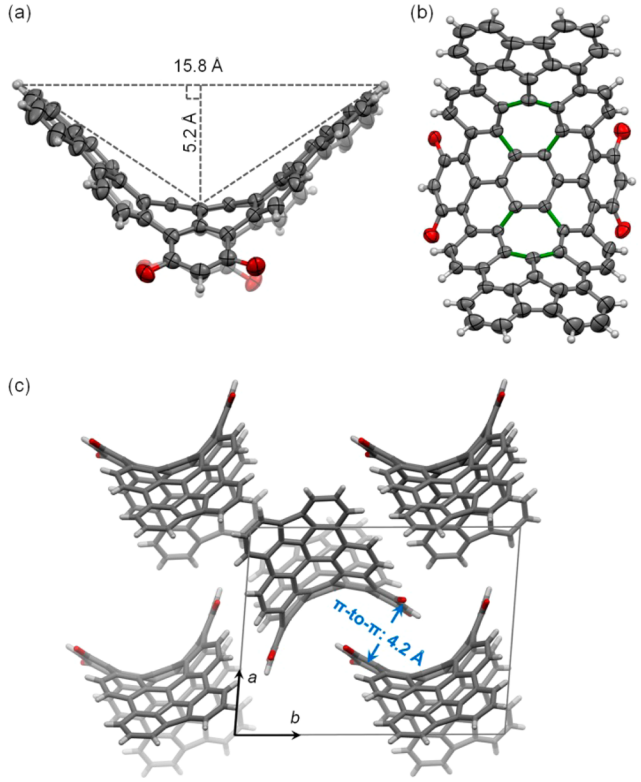

Figure 4. Crystal structure of **1b**: (a) side view and (b) top view of the π-backbone of **1b** with the hexyl groups removed and carbon atom positions shown as 50% probability ellipsoids; (c) molecular packing of **1b** as viewed along the *c* axis of the unit cell. (Alkyl groups and crystallized water molecules are removed for clarity.)

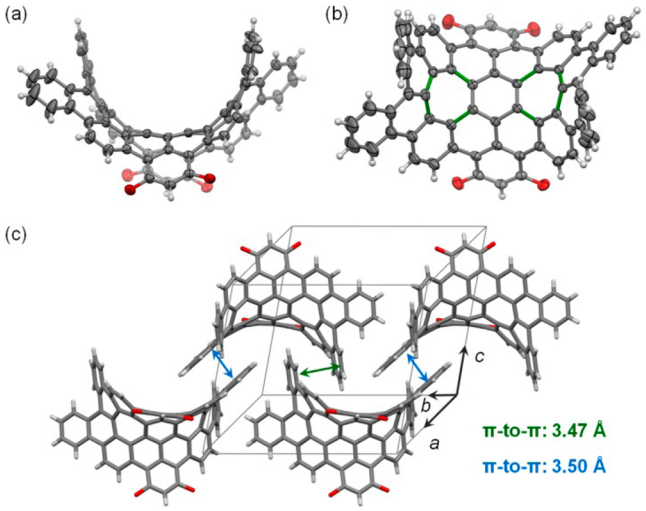

Figure 5. Crystal structure of **2b**: (a) side view and (b) top view of the π-backbone of **2b** with the hexyl groups removed and carbon atom positions shown as 50% probability ellipsoids; (c) molecular packing of **2b** with the unit cell. (Alkyl groups are removed for clarity.)

individual rings is defined as the average distance of the carbon atoms in a ring from a generated best-fit plane.[18] Therefore, a more curved ring is associated with a larger value of nonplanarity. HOMA is a quantitative measure of aromaticity based on bond length as defined by

$$\mathrm{HOMA} = 1 - \frac{\alpha}{n}\sum (R_{\mathrm{opt}} - R_i)^2$$

where n is the number of bonds taken into the summation, α is an empirical constant chosen to give HOMA = 0 for the hypothetical Kekulé structures of the typical aromatic systems with alternation of single and double bonds and HOMA = 1 for the system with all bond lengths equal to the optimal value R_{opt}, and R_i is the individual bond length in the ring.[17] Therefore, a typical aromatic ring has a HOMA value of 1, and a smaller HOMA value is associated with lower aromaticity.

As shown in Table 1, the most curved rings in both **1b** and **2b** are the seven-membered rings (G) in terms of the nonplanarity.

Table 1. Analysis of HOMA and Nonplanarity for each Ring in 1b and 2b

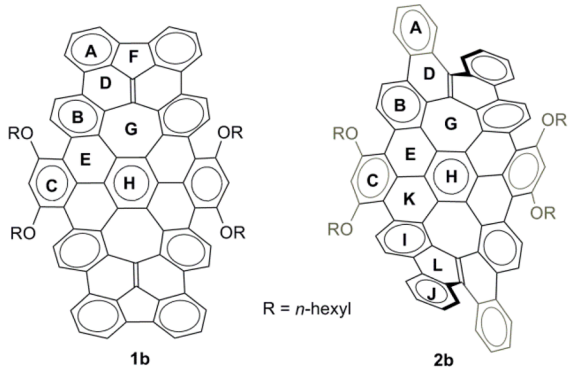

	nonplanarity[a]		HOMA[b]	
ring	1b	2b	1b	2b
A	0.019	0.007	0.871	0.893
B	0.048	0.038	0.639	0.756
C	0.043	0.034	0.926	0.928
D	0.037	0.064	0.278	0.320
E	0.143	0.125	0.250	0.212
F	0.017		0.277	
G	0.185	0.229	−0.229	−0.142
H	0.102	0.104	0.711	0.808
I		0.068		0.829
J		0.025		0.937
K		0.135		0.329
L		0.128		0.269

[a]Planarity values were calculated by constructing a best-fit plane through the individual rings and measuring the average distance of the carbon atoms from this plane. [b]HOMA values were calculated by using the normalization constant (α) of 257.7 and the optimal bond length (R_{opt}) of 1.388 Å.

In contrast, the five-membered rings (F) in **1b** are essentially flat. With the nonplanarity larger than 0.1, rings E and H in **1b** are more curved than other six-membered rings. The most curved rings in **1b**, G and E, involve dihedral (torsion) angles as large as 44.3° and 31.9°, respectively. In **2b**, rings E, H, K, and L are more curved than other six-membered rings with the nonplanarity larger than 0.1. The rings D and L in **2b** are more distorted than ring D in **1b**, in agreement with the helical structure of [4]helicene moiety. The most curved rings in **2b**, G and K, involve dihedral (torsion) angles as large as 46.0° and 33.2°, respectively.

As shown in Table 1, ring C in **1b** has the highest value of HOMA (0.926) followed by rings A, H, and B with HOMA values higher that 0.63 while rings D and E in **1b** have significantly lower HOMA values (0.278 and 0.250). Ring J in **2b** has the highest value of HOMA (0.937) followed by rings C, A, I,

DOI: 10.1021/jacs.5b00403
J. Am. Chem. Soc. 2015, 137, 3910−3914

H, and B with HOMA values higher that 0.75, while rings D, E, K, and L in **2b** have HOMA values lower than 0.33. The higher HOMA values of rings A, B, C, H, I, and J can be correlated with aromatic sextets as shown in the molecular structures in Table 1 following Clar's rule.[19] In contrast, rings E and K are "empty", and rings D and L contain a double bond. Therefore, they are much less aromatic. Another finding from Table 1 is that the planarity roughly correlates with the aromaticity. The six-membered rings with lower HOMA have a better chance to be bent in the curved π-backbone.

Semiconductor Properties. To explore the potential of saddle-shaped polycyclic arenes as semiconductors, we tested **1b**, **2b**, and **3b**, three molecules with different polycyclic frameworks but the same alkyl side chain, in solution-processed thin film transistors. To fabricate thin films, a solution of **1b**, **2b**, or **3b** in THF was drop-cast onto a silicon wafer, whose SiO_2 surface was pretreated with a self-assembled monolayer of octadecyltrimethoxysilane (OTMS).[20] The as-cast films were then annealed at 60 °C for 10 min. As found from X-ray diffraction, the film of **2b** appeared amorphous while the films of **1b** and **3b** were polycrystalline. The transistors were completed by depositing a layer of gold onto the organic films through a shadow mask to form top contact source and drain electrodes. As measured in ambient air from these devices, **1b** and **3b** functioned as p-type semiconductors with field effect mobilities of 1.3×10^{-5} and 6×10^{-4} cm^2 V^{-1} s^{-1}, respectively. In contrast, the films of **2b** behaved as an insulator without any field effect although its crystal structure exhibits the best $\pi-\pi$ interactions among the three molecules. This can be attributed to the amorphous film of **2b**, which lacks long-range order to allow effective charge transport in channels of about 100 μm long. The low field effect mobilities of **1b** and **3b** are likely related to the very limited $\pi-\pi$ interactions in the solid state as well as the poor film morphology as found with atomic force microscopy.

CONCLUSION

We have demonstrated that saddle-shaped ketone **3c**, which has two tropone subunits embedded in the well-known framework of HBC, is a useful precursor for synthesis of large aromatic saddles by reactions on the carbonyl groups. Derivatives (**1a**,**b** and **2a**,**b**) of two novel aromatic saddles ($C_{70}H_{26}$ and $C_{70}H_{30}$) were successfully synthesized from **3c** in two ways. On the basis of crystal structures, local aromaticity and nonplanarity of individual rings in the saddle-shaped π-backbone of **1b** and **2b** were analyzed, and were found to follow Clar's rule in general.[19] Moreover, as found from a preliminary study on semiconductor properties, **1b** and **3b** functioned as p-type semiconductors in solution-processed thin film transistors while **2b** behaved as an insulator. Connecting two molecules of **3a**–**c** with suitable linking groups can in principle lead to a conjugated nanoring. Experiments to test this idea are in progress in our laboratory.

ASSOCIATED CONTENT

Supporting Information

Details of synthesis and characterization, the crystallographic information files (CIF) for **1b**, **2b**, and **3b**, fabrication, and characterization of organic thin film transistors, NMR spectra. This material is available free of charge via the Internet at http://pubs.acs.org.

AUTHOR INFORMATION

Corresponding Author

miaoqian@cuhk.edu.hk

Notes

The authors declare no competing financial interest.

ACKNOWLEDGMENTS

We thank Ms. Hoi Shan Chan (the Chinese University of Hong Kong) for the single crystal crystallography. This work was supported by the Research Grants Council of Hong Kong (Project No.: GRF402412) and the University Grants Committee of Hong Kong (Project No.: AoE/P-03/08).

REFERENCES

(1) Chuang, C.; Fan, Y.-C.; Jin, B.-Y. *J. Chem. Inf. Model.* **2009**, *49*, 361–368.
(2) Bharat; Bhola, R.; Bally, T.; Valente, A.; Cyrański, M. K.; Dobrzycki, Ł.; Spain, S. M.; Rempała, P.; Chin, M. R.; King, B. T. *Angew. Chem., Int. Ed.* **2010**, *49*, 399–402.
(3) Rieger, R.; Müllen, K. *J. Phys. Org. Chem.* **2010**, *23*, 315–325.
(4) Lenosky, T.; Gonze, X.; Teter, M.; Elser, V. *Nature* **1992**, *355*, 333–335.
(5) Iijima, S.; Ichibashi, T.; Ando, Y. *Nature* **1992**, *356*, 776–778.
(6) Park, N.; Yoon, M.; Berber, S.; Ihm, J.; Osawa, E.; Tománek, D. *Phys. Rev. Lett.* **2003**, *91*, 237204–1/4.
(7) Beuerle, F.; Herrmann, C.; Whalley, A. C.; Valente, C.; Gamburd, A.; Ratner, M.; Stoddart, J. F. *Chem.—Eur. J.* **2011**, *17*, 3868–3875.
(8) For recent examples of saddle-shaped polycylic arenes containing octagons or heptagons, see: (a) Sakamoto, Y.; Suzuki, T. *J. Am. Chem. Soc.* **2013**, *135*, 14074–14077. (b) Feng, C.-H.; Kuo, M.-Y.; Wu, Y.-T. *Angew. Chem., Int. Ed.* **2013**, *52*, 7791–7794. (c) Pradhan, A.; Dechambenoit, P.; Bock, H.; Durola, F. *J. Org. Chem.* **2013**, *78*, 2266–2274.
(9) Luo, J.; Xu, X.; Mao, R.; Miao, Q. *J. Am. Chem. Soc.* **2012**, *134*, 13796–13803.
(10) Kawasumi, K.; Zhang, Q.; Segawa, Y.; Scott, L. T.; Itami, K. *Nat. Chem.* **2013**, *5*, 739–744.
(11) Wu, J.; Pisula, W.; Müllen, K. *Chem. Rev.* **2007**, *107*, 718–747.
(12) Rigaudy, J.; Nedelec, L. *Bull. Soc. Chim. Fr.* **1959**, 655–659.
(13) Ried, W.; Ehret, J. *Angew. Chem., Int. Ed.* **1968**, *7*, 377–378.
(14) Leung, N. L. C.; Xie, N.; Yuan, W.; Liu, Y.; Wu, Q.; Peng, Q.; Miao, Q.; Lam, J. W. Y.; Tang, B. Z. *Chem.—Eur. J.* **2014**, *20*, 15349–15353.
(15) The commonly used formal potential of the redox couple of ferrocenium/ferrocene (Fc+/Fc) in the Fermi scale is −5.1 eV, which is calculated on the basis of an approximation neglecting solvent effects using a work function of 4.46 eV for the normal hydrogen electrode (NHE) and an electrochemical potential of 0.64 V for (Fc+/Fc) versus NHE. See: Cardona, C. M.; Li, W.; Kaifer, A. E.; Stockdale, D.; Bazan, G. C. *Adv. Mater.* **2011**, *23*, 2367–2371.
(16) Anslyn, E. V.; Dougherty, D. A.; *Modern Physical Organic Chemistry*; University Science Books: Sausalito, CA, 2004; Chapter 1, p 22.
(17) (a) Kruszewski, J.; Krygowski, T. M. *Tetrahedron Lett.* **1972**, 3839–3842. (b) Krygowski, T. M. *J. Chem. Inf. Comput. Sci.* **1993**, *33*, 70–78. (c) Krygowski, T. M.; Cyrański, M. K. *Chem. Rev.* **2001**, *101*, 1385–1419.
(18) The average distance of the carbon atoms in a ring from a generated best-fit plane was used to evaluate the nonplanarity of a ring in polycyclic arenes, but was named as *planarity*. See: Miller, R. W.; Duncan, A. K.; Schneebeli, S. T.; Gray, D. L.; Whalley, A. C. *Chem.—Eur. J.* **2014**, *20*, 3705–3711.
(19) Clar, E. *The Aromatic Sextet*; Wiley: New York, 1972.
(20) Ito, Y.; Virkar, A. A.; Mannsfeld, S.; Oh, J. H.; Toney, M.; Locklin, A.; Bao, Z. *J. Am. Chem. Soc.* **2009**, *131*, 9396–9404.

DOI: 10.1021/jacs.5b00403
J. Am. Chem. Soc. 2015, 137, 3910–3914